frontiers in Physics

MINI REVIEW
published: 30 August 2021
doi: 10.3389/fphy.2021.726996

Polarization-Sensitive Second Harmonic Generation Microscopy for Investigations of Diseased Collagenous Tissues

*Richard Cisek, Ariana Joseph, MacAulay Harvey and Danielle Tokarz**

Department of Chemistry, Saint Mary's University, Halifax, NS, Canada

The advancement of non-invasive quantitative optical diagnosis techniques such as polarization-sensitive second harmonic generation microscopy (PSHG) for diseases such as cancer presents opportunities for improving disease understanding and survival rates. Here, novel and developing techniques in PSHG microscopy applied for the differentiation of cancerous or diseased tissues are presented, including circular dichroism, modulation of laser linear polarization, detection of outgoing linear laser polarization, and double-Stokes Mueller. Typically, initial cancer diagnosis is performed by visual inspection of stained biopsy or surgical resection tissue sections under bright-field microscopy, however, early diagnosis is challenging due to variability in morphological interpretation of the tissues, and because cancer initiation regions can be small and easy to miss. Therefore, pathologists could benefit in identifying cancer on biopsy or surgical resection sections by using unbiased quantitative automated technologies with high spatial resolution and improved disease specificity that can check the entire slide pixel-by-pixel. Second harmonic generation microscopy offers the opportunity to measure ultrastructural alterations in collagenous scaffolds of organ tissues virtually background free on submicron-sized tissue regions. The approach is particularly interesting for cancer diagnosis applications, because during cancer initiation and progression, the collagen in the affected tissue extracellular matrix is often deregulated and becomes disorganized. This mini-review contains a thorough summary of PSHG techniques that have interrogated diseased tissues, and discusses their technical variations and successes in disease discrimination.

Keywords: cancer, optical pathology, medical imaging, nonlinear optical polarimetry, nonlinear optical microscopy

OPEN ACCESS

Edited by:
Nirmal Mazumder, Manipal Academy of Higher Education, India

Reviewed by:
Stefan G. Stanciu, Politehnica University of Bucharest, Romania
Mehdi Alizadeh, Vilnius University, Lithuania
Francisco Avila, Universidad de Zaragoza de, Spain

****Correspondence:***
Danielle Tokarz
danielle.tokarz@smu.ca

Specialty section:
This article was submitted to Optics and Photonics, a section of the journal Frontiers in Physics

Received: *17 June 2021*
Accepted: *10 August 2021*
Published: *30 August 2021*

Citation:
Cisek R, Joseph A, Harvey M and Tokarz D (2021) Polarization-Sensitive Second Harmonic Generation Microscopy for Investigations of Diseased Collagenous Tissues. Front. Phys. 9:726996. doi: 10.3389/fphy.2021.726996

INTRODUCTION

Second harmonic generation (SHG) or frequency doubling is a nonlinear optical process which occurs efficiently in a microscope when two laser photons of wavelength λ interact with matter to produce light at $\lambda/2$ (**Figure 1B**). Only non-central symmetric materials at both molecular and macromolecular scales can produce SHG and therefore, microcrystalline structures are required for SHG. In animals, most SHG occurs from fibrous collagenous connective tissues or myosin in muscle tissues, both having a non-central microcrystalline structure. Since the SHG is emitted due to the presence and ultrastructure of the muscle or collagen interacting with the laser, no dyes or

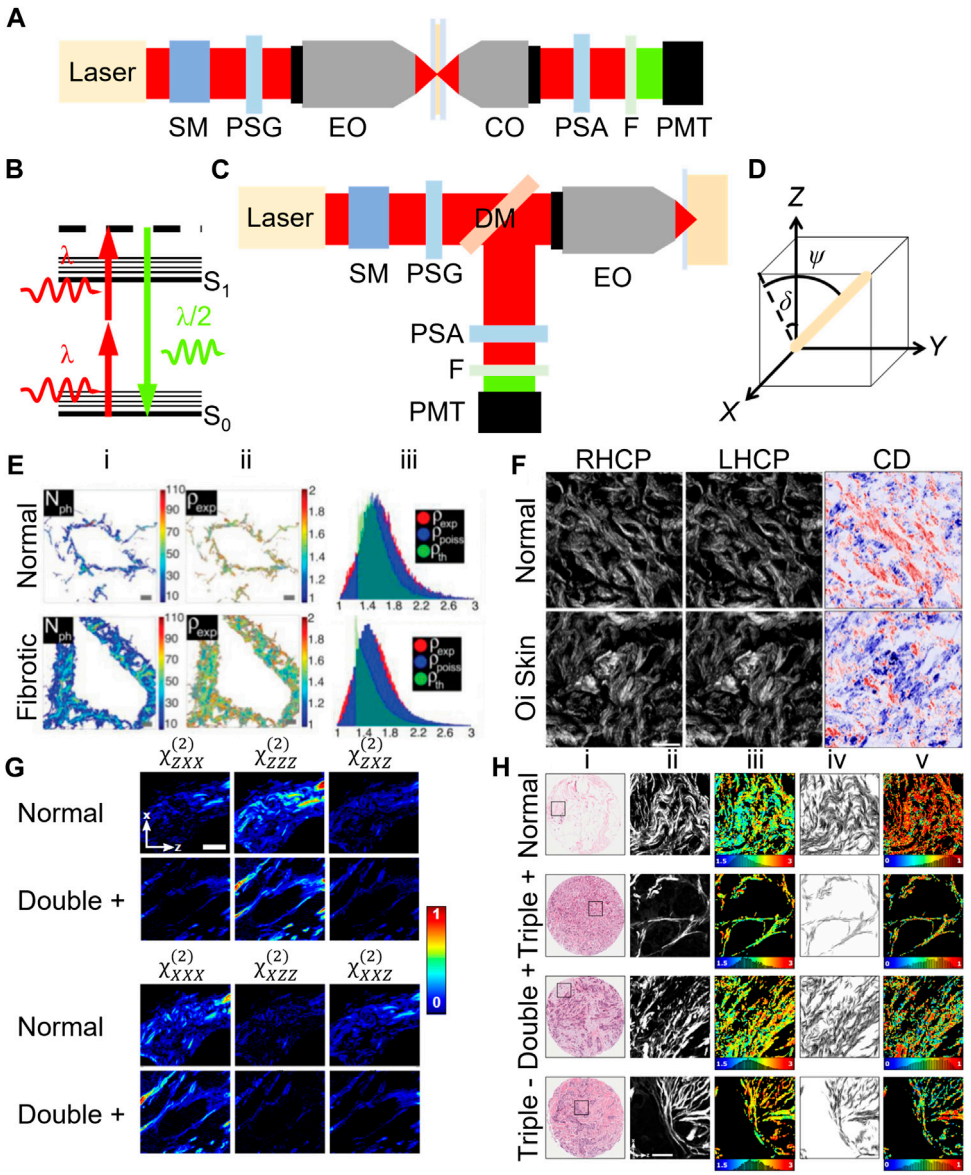

FIGURE 1 | Typical microscope schematics for forward- **(A)** and epi-detection **(C)** configurations for polarization-sensitive second harmonic generation (SHG) microscopy. The energy state diagram of SHG **(B)** along with the coordinate system, where Z-X is the image plane and the laser propagates along Y, for an arbitrarily oriented fiber **(D)** is shown. Abbreviations: SM-scanning mirrors, PSG-polarization state generator, EO-excitation microscope objective, CO-collection microscope objective, PSA-polarization state analyzer, F-filter, PMT-photomultiplier tube detector and DM-dichroic mirror. Example images obtained using PI-SHG **(E)**, CD-SHG **(F)**, DSMP-SHG **(G)** and PIPO-SHG **(H)**. SHG intensity (E-i), fitted ρ (E-ii) and fitted ρ distribution width (E-iii) are shown for normal and fibrotic liver [14]. SHG images **(F)** of normal skin and osteogenesis imperfecta (O-i) skin tissues using right-handed circularly polarized light (RHCP), left-handed circularly polarized light (LHCP) and CD-SHG (CD) where red and blue show positive and negative values, respectively [43]. Laboratory-frame $\chi^{(2)}$ values **(G)** of normal and double + breast tissue using DSMP-SHG [44]. Brightfield (H-i), SHG (H-ii), ρ (H-iii), δ orientation (H-iv) and DOLP (H-v) images of normal, triple +, double +, ++-, and triple–breast tissue [44]. Images E-H were adapted with permission from [14, 43, 44] © The Optical Society.

sample modification procedures are needed, and the signal can be interpreted as a direct indicator of structural sample changes.

SHG is energy conserving and consequently does not photobleach, differing significantly from non-parametric processes, such as fluorescence, where absorbed Stokes energy often leads to sample damage and photobleaching. For biological imaging, lasers with wavelength outside of the tissue absorption spectrum are typically chosen, therefore reduced heat is deposited into the sample allowing for long duration functional *in vivo* studies.

The SHG intensity and polarization can be written: $\vec{I}_{SHG} \propto \chi^2 : \vec{E}\vec{E}$, where ":" is the tensor product, $\vec{E}$ is the intensity and polarization of the laser electric field, and $\chi^{(2)}$

is the second-order nonlinear optical susceptibility tensor, containing up to 18 unique elements, describing the sample. The equation shows that intensity and polarization of SHG depends on the sample orientation and ultrastructure, encoded in $\chi^{(2)}$, and on the polarization and intensity of the laser. Kleinman symmetry [1, 2], where $K = \chi^{(2)}_{zxx}/\chi^{(2)}_{xxz} = 1$, as well as cylindrical C_{6v} symmetry are typically assumed, resulting in only two unique $\chi^{(2)}$ elements whose ratio is historically designated $\rho = \chi^{(2)}_{zzz}/\chi^{(2)}_{zxx}$ [3]. Since $\vec{E}$ is controlled and $\vec{I}_{SHG}$ is measured, ρ, and the in-plane projection of the orientation angle of collagen, δ, can be extracted via PSHG measurements (see **Figure 1D** for coordinate system). This review is focused on polarization-sensitive SHG approaches specifically used for discriminating diseased collagenous tissues, and thus many great papers using SHG microscopy are regretfully not included.

Historical Interpretation of the PSHG Parameters Pertaining to Collagen

Researchers, Freund et al. [3–6], pioneered the use of SHG to investigate the structure of collagenous biological tissue by utilizing different laser polarizations. They focused a Q-switched Nd:YAG laser onto rat tail tendon, collecting SHG in the forward direction, similar to **Figure 1A**, but without scan mirrors and at different scattering angles. They found an SHG peak at the 0° scattering angle, indicative of the macroscopic ordered polar structure of collagen, and found that $\chi^{(2)}$ of tendon exhibited cylindrical symmetry, since rotation about the tendon axis did not appreciably change SHG parameters. They attributed the signal predominantly to C-N bonds in the amino acids, arguing these are the likely dominant polarizable, noncentrosymmetric and non-mobile candidates. They used a polarization state analyzer (PSA) consisting of a polarizer to directly measure ρ for tendons from rats of different age groups, and showed this parameter distinguishes the variation in the developing biological structure.

Noting the important SHG theoretical work of Dick [7], two groups, Plotnikov et al. [8] and Tiaho et al. [9], attributed ρ to the helical pitch (θ) of the protein triple helix via $\rho/(2+\rho) = \cos\theta$. However, it is likely that all the levels of the collagen tissue hierarchy can contribute to the polarization-dependent SHG parameters [10]. Therefore, the question of which hierarchical levels of collagen in different tissues are expressed in PSHG microscopy remains open. It also presents an opportunity to investigate which disease states affect the quantitative imaging results. Since the dyes used for standard staining of histopathology samples in hospitals, hematoxylin and eosin Y, seem to be compatible with PSHG microscopy [10], therefore PSHG capability could be added to existing histopathology slide scanners enabling the new modality without altering standard hospital sample preparation procedures. The resulting automated quantitative analysis could yield pathologists with an additional quantitative marker for improved diagnosis and evaluation.

APPLICATIONS OF SHG MICROSCOPY FOR DETERMINING THE ULTRASTRUCTURE OF DISEASED COLLAGENOUS TISSUES

Polarization-In SHG Microscopy

Pioneered in 1979, polarization-in SHG (PI-SHG) microscopy utilizes a polarization state generator (PSG) to rotate the laser linear polarization state. One method is to use a half-wave plate (HWP) in a motorized rotating mount, located before the excitation objective lens (**Figures 1A,C**). An SHG intensity image is recorded at each HWP angle, typically with 10–30 steps in the range 0°–90°. Since SHG is predominantly forward-directed, most epi-detected photons require backscattering, which is less efficient than forward-detection [11], and results in depolarization of a fraction of the SHG. Parameters ρ and δ can be found using this methodology by performing nonlinear data fitting.

PI-SHG microscopy was used to distinguish normal and diseased tissue regions in several tissues (**Table 1**) with statistical significance, via the $\chi^{(2)}_{zzz}$ values of osteosarcoma, breast cancer and melanoma tissues [12], as well as the ρ and θ values of fibrotic and control liver vessels [13, 14]. A significant increase in the ρ value was also found between breast cancer biopsy tissues [15, 16], and during thermal denaturation of corneal stroma [17]. Several other studies were performed using this technique, including on liver fibrosis [18], osteoarthritis [19], and keratoconus [20, 21].

To avoid delays due to nonlinear data fitting, a fast Fourier transform (FFT) algorithm has been developed to extract ρ values quickly [22]. It was used in the study of normal and keratoconic human corneas [23], human breast carcinoma samples [16, 24] and to investigate mechanical load in energy storing versus positional collagen fibrils [25]. The FFT approach has also allowed use of a generic structural model, where rather than assuming a particular symmetry, the second-order FFT coefficients (I_2 and ϕ_2), which quantify the modulation depth of the polarization SHG response (I_2) and its phase (ϕ_2), are reported and compared. This approach was used for a survey on cartilage in osteo-arthritic tissue [26, 27], for a study of ageing via investigating ribose-glycated fibrils isolated from rat tail [28], and to investigate needle puncture damage in bovine annulus fibrosus [29].

Several groups have also investigated the excitation anisotropy (α) for distinguishing diseased tissues, $\alpha = I_v - I_H/I_v + I_H$, where I_v and I_H are the SHG intensities when the incident light is vertically and horizontally polarized, respectively. α is related to δ, and was measured in skin exposed to UVB [30, 31], and using a fast motion-artefact free implementation in cheek and eye corner skin at two ages [32].

Polarization analysis of the outgoing SHG has also been incorporated using a PSA typically located after the collection objective in a forward-detection geometry (**Figure 1A**), or after a dichroic mirror that separates SHG in epi-detection (**Figure 1C**). While variable PSAs are reviewed in *Double Stokes Mueller Polarimetric SHG (DSMP-SHG) Microscopy*

TABLE 1 | A summary of the PSHG microscopy techniques used for quantifying the differences in collagen structure in diseased tissue and the corresponding parameters measured with those techniques. The following abbreviation is used NR: Not reported.

Technique	Condition	Parameters: Statistical significance	References
PI-SHG	Osteosarcoma, Breast cancer and Melanoma	$\chi^{(2)}_{zzz}$: Yes, β: NR	[12]
PI-SHG	Liver fibrosis	ρ: Yes, θ: Yes	[13, 14]
PI-SHG	Mammary dysplasia and breast cancer	K: Yes, ρ: Yes, $\chi^{(2)}_{xxx}/\chi^{(2)}_{zxx}$: Yes	[15]
PI-SHG	Breast ductal carcinoma	β: Yes, ρ: Yes	[16]
PI-SHG	Thermal denaturation	θ: Yes	[17]
PI-SHG	Liver fibrosis	ρ: NR, $\chi^{(2)}_{xxz}/\chi^{(2)}_{zxx}$: NR	[18]
PI-SHG	Osteoarthritis	Polarization plots: NR	[19]
PI-SHG	Keratoconus	Polarization plots: NR	[20]
PI-SHG	Keratoconus	δ: No	[21]
PI-SHG	Keratoconus	θ: NR, δ: NR	[23]
PI-SHG	Breast carcinoma	ρ: Yes	[24]
PI-SHG	Mechanical load	ρ: Yes	[25]
PI-SHG	Osteoarthritis	I_2 and ϕ_2: NR	[27]
PI-SHG	Aged	I_2 and ϕ_2: Yes	[28]
PI-SHG	Needle puncture damage	I_2: No	[29]
PI-SHG	UVB exposure	α : Yes	[30, 31]
PI-SHG	Aged	δ: NR	[32]
PI-SHG	Skin dysplasia	β: NR	[33]
PI-SHG	Aged	β: Yes	[34]
PI-SHG	Osteogenesis imperfecta	β: No	[35]
PI-SHG	Colorectal dysplasia and cancer	β: Yes	[36]
PI-SHG	Ovarian cancer	β: NR	[37]
PI-SHG	Mechanical load	ρ: Yes	[38]
PI-SHG	Irradiation	ρ: Yes	[39]
PI-SHG	CT26 derived tumor from mice	ρ: NR, θ: NR	[40]
PI-SHG	Implantation of B16 melanoma cells	ρ: NR, θ: NR	[40]
PI-SHG	Implantation of CT26 colon carcinoma cells and 4T1 breast cancer cells	ρ: NR, θ: NR	[41]
PI-SHG	Esophageal squamous cell carcinoma	ρ: No	[42]
PI/CD-SHG	Ovarian cancer	θ: Yes, β (0°): Yes, $I_{CD\text{-}SHG}$: Yes	[49]
CD-SHG	Osteogenesis imperfecta	$I_{CD\text{-}SHG}$: Yes	[43]
CD-SHG	Idiopathic pulmonary fibrosis	θ: No, $I_{CD\text{-}SHG}$: Yes	[47]
CD-SHG	3D spheroid models of idiopathic pulmonary fibrosis	θ: Yes, $I_{CD\text{-}SHG}$: Yes	[48]
DSMP-SHG	Breast cancer with ER, PgR and HER2 expression	K: No, $\chi^{(2)}_{zzz}$, $\chi^{(2)}_{zxx}$, $\chi^{(2)}_{zxz}$, $\chi^{(2)}_{xxx}$, $\chi^{(2)}_{xzz}$, and $\chi^{(2)}_{xxz}$: NR	[44]
PIPO-SHG	Breast cancer with ER, PgR and HER2 expression	ρ: Yes, DOLP: Yes	[44]
PIPO-SHG	Thyroid carcinomas and diseases	ρ: Yes, C: No, DOLP: Yes	[55, 58, 59]
PIPO-SHG	Non-small cell lung carcinoma	ρ: Yes, C: Yes, DOLP: Yes, δ: Yes	[56]
PIPO-SHG	Non-small cell lung carcinoma	ρ: Yes	[57, 58]
PIPO-SHG	Pancreatic ductal adenocarcinoma	ρ: Yes, C: Yes, DOLP: Yes	[58, 60]
PIPO-SHG	Bone cancer	ρ: Yes	[61]
PO-SHG	Breast cancer	θ: No	[62]
PO-SHG	Atherosclerosis	ρ: No	[63]

and *Polarization-In, Polarization-Out SHG (PIPO-SHG) Microscopy* sections, stationary PSAs are also used. In one implementation, SHG intensity through a polarizer parallel ($I_{||}$) and perpendicular ($I_{\perp}$) to the laser linear polarization is recorded allowing the SHG anisotropy (β) to be calculated: $\beta = I_{||} - I_{\perp}/I_{||} + 2I_{\perp}$. A study of dysplastic human skin showed that optimization of the selection of linear laser polarization orientations using a Fourier algorithm on the SHG intensity obtained with circularly polarized light allowed β values to distinguish diseased areas more effectively [33], while in rat skin, β significantly changed during ageing [34]. In another study, the β values of femurs from wild-type mice and oim mice, a model for human osteogenesis imperfecta, were similar [35] while different β values are reported for dysplasia and colon cancer [36] as well as ovarian cancer tissue [37]. Stationary PSAs where the collagen axis is aligned to the laboratory polarization axis have also been used for investigating effects of mechanical load [38] and irradiation with high intensity infra-red light [39].

Interestingly, analysis of the PSHG data has also been achieved through Fourier projection of the PSHG image stacks onto two phasor plots referred to as microscopic multiparametric analysis by phasor projection of PSHG (μMAPPS). This technique has been used to compare the ρ values of SHG data taken from biopsies of the left flank of mice days after implantation of melanoma [40], colon carcinoma and breast cancer cells [41].

PI-SHG microscopy was also used to image submucosa of esophageal squamous cell carcinoma (ESCC). The ρ values from 4 stages of ESCC showed few differences between one another, and

authors concluded that PI-SHG microscopy cannot be used for staging ESCC because the structural changes are likely of macromolecular rather than micromolecular origin [42].

Circular Dichroism Second Harmonic Generation Microscopy

In circular dichroism SHG (CD-SHG) microscopy, two SHG images are obtained using left-handed (I_L) and right-handed (I_R) circularly polarized laser light, with no PSA in the SHG detection path (**Figures 1A,C**). The CD-SHG intensity ($I_{CD\text{-}SHG}$) is the normalized difference of the two quantities, $I_{CD-SHG} = 2(I_L - I_R)/(I_L + I_R)$. One way to implement CD-SHG is via a liquid-crystal rotator (LCR) followed by a quarter-wave plate (QWP) as the PSG [45]. $I_{CD\text{-}SHG}$ is a complicated parameter when expressed in terms of the sample susceptibility, and according to equation 12 in [46], only measures structures with nonzero chirality ($\chi^{(2)}_{xyz}$), nonzero phase between $\chi^{(2)}$ elements, and nonzero angle to the imaging plane (ψ in **Figure 1D**). Nonzero phase between tensor elements can occur due to a resonance transition near the laser wavelength and/or the SHG wavelength, due to a molecular magnetic dipole or due to an electric quadrupole rather than dipolar interaction [46].

CD-SHG microscopy was applied to determine differences between normal and osteogenesis imperfecta skin tissues as well as idiopathic pulmonary fibrosis human lung tissue where variations in $I_{CD\text{-}SHG}$ were statistically significant [43, 47, 48]. Another study used CD-SHG microscopy to find differences between 4 ovarian tissue classifications. The mean $I_{CD\text{-}SHG}$ value for normal ovarian tissue was significantly higher than the other tissues [49].

Double Stokes Mueller Polarimetric SHG Microscopy

Double Stokes Mueller polarimetric SHG (DSMP-SHG) microscopy, introduced in 2015 [50, 51], is an alternative method to performing PSHG microscopy. DSMP-SHG microscopy aims to obtain all possible polarization information in the smallest amount of measurements. Stokes vectors are used to describe the laser polarization ($\vec{s}$) and polarization of the SHG signal ($\vec{s}\,'$). Their relation is described by the function $\vec{s}\,' = \mathcal{M}\,\vec{s}$, where $\mathcal{M}$ is a double Mueller matrix which can be characterized via measurement. One such implementation using a single detector required 54 measurements. A PSG produced linearly polarized states at angles 0°, ±45°, 90°, 157.5°, two elliptical states, and two circularly polarized states, while at each PSG state, 6 SHG polarization intensities are measured to obtain a Stokes vector using the PSA. Both the PSG and PSA consisted of a polarizer, HWP and QWP at the laser and SHG wavelengths, respectively, with waveplates in mechanical rotation mounts (**Figures 1A,C**) [44].

DSMP-SHG has the advantage that 6 laboratory frame susceptibility components can be extracted from double Mueller matrix components: $\chi^{(2)}_{xxx}$, $\chi^{(2)}_{xzz}$, $\chi^{(2)}_{xxz}$, $\chi^{(2)}_{zxx}$, $\chi^{(2)}_{zzz}$, $\chi^{(2)}_{zxz}$ (calculated relative to one component), and for each component, the real (**Figure 1G**) and imaginary parts can be extracted, for each pixel of the image. **Figure 1G** can be used to compare tensor components for each pixel of the image [44]. Additionally, one can obtain the degree of polarization (DOP), degree of linear polarization (DOLP) and degree of circular polarization (DOCP) at each input polarization. DSMP-SHG microscopy was used to study microarray slides of human breast cancer types, finding that components of $\chi^{(2)}$ are predominantly real and validating Kleinman symmetry [44]. When the $\chi^{(2)}$ components are real and birefringence is negligible, the polarization of the SHG signal will not have a circular component, hence a reduced polarimetric measurement with only linearly polarized incoming and outgoing states known as polarization-in, polarization-out SHG microscopy can be performed [50–52].

Polarization-In, Polarization-Out SHG Microscopy

Polarization-in, polarization-out SHG (PIPO-SHG) uses a simplified PSA compared to DSMP-SHG as well as the same PSG as in the PI-SHG technique, and hence is typically implemented using a forward-detection geometry (**Figure 1A**). The PSA measures the linear polarization state of the SHG signal at different angles of the linear polarization of the laser. The simplest PSA consists of a linear polarizer in a motorized rotation mount. SHG images are typically captured with at least 8 PSG angles and 8 PSA angles, hence at least 64 images are recorded for the technique, resulting in ~20 min acquisition times in comparison to PI-SHG which takes ~1.5 min [53]. The additional dimensionality of the data is thought to produce higher accuracy fitting, although at the time of writing this manuscript no study has performed the comparison with the other techniques. Fitting of the SHG intensity versus PSA and PSG angles yields δ and ρ. When the more generalized C_6 symmetry is assumed, $\chi^{(2)}_{xyz}$ appears, and can be measured as the chirality ratio ($C = \chi^{(2)}_{xyz}/\chi^{(2)}_{zxx}$) [54].

The PIPO-SHG measurements also allow the DOLP of the SHG signal to be obtained, where the SHG light is fully linearly polarized when $DOLP = 1$, and increasingly depolarized or circularly polarized as it approaches 0. DOLP measurements were performed at 8 incident laser polarizations (θ = 0°, 22.5°, 45°, 67.5°, 90°, 112.5°, 135°, 157.5°) and for each one, two DOLP calculations were averaged, one using measurements at analyzer angles 0°, 45°, 90°, 135° and another at 22.5°, 67.5°, 112.5°, 157.5° [55]. An improved DOLP is obtained when structures with δ orientations closest to the normal of the crystal axis are ignored, since they have the lowest signal in collagen imaging, which can result in a low signal-to-noise ratio [44]. Lower DOLP values can occur due to ultrastructural disorder of collagen, or due to fragmentation of collagen within the focal volume, where SHG is emitted from uncorrelated domains [56].

A PIPO-SHG microscopy study of pathology slides of lung samples from patients with non-small cell lung carcinoma revealed significant differences in the mean ρ values [57]. A

more recent study of that disease showed that the median ρ and the median average distribution (MAD) of δ could differentiate stages II and III from normal tissue, while the MAD of C and DOLP could differentiate stage I [56]. Human thyroid tissues were also investigated with PIPO-SHG, and revealed significant differences in the average DOLP values between normal thyroid tissue and follicular variant of papillary thyroid carcinoma, classical papillary thyroid carcinoma, follicular nodular disease, Grave's disease, and anaplastic or undifferentiated carcinoma. This was also true for the mean ρ values except for insular thyroid tissues [58, 59]. Pancreatic ductal adenocarcinoma tissue was also investigated with PIPO-SHG and demonstrated significant differences between the mean ρ values of tumor tissue and the periductal, lobular and parenchymal regions of normal pancreatic tissue. The DOLP values of the pancreatic tumor regions were only significantly different from normal periductal and parenchymal tissues [60] while the C values in diseased thyroid and pancreas were not significantly different from normal tissues [58–60].

PIPO-SHG microscopy was also applied to study a microarray slide containing 3 pathological human breast cancer types (**Figure 1H**) with the overexpression/absence of estrogen receptor, progesterone receptor, and human epidermal growth factor receptor 2: triple +, double +, and triple -. The mean and median ρ values of triple + and double + as well as the mean and median DOLP values for double + were significantly different from normal breast tissue [44]. Bone cancer was also investigated and the ρ values of bone adjacent to tumor was found to be significantly different to bone adjacent to normal marrow [61]. Polarization-out SHG (PO-SHG) microscopy was also attempted by varying the angle of an analyzer before the detector, as in PIPO-SHG, but with only one linear input polarization state, however, it did not achieve differentiation between normal and diseased tissue [62, 63].

DISCUSSION

Automated digital histopathology using PSHG microscopy is a promising technology for diagnosis of disease in histopathological samples, however, implementation requires fast imaging and data analysis balanced with maintaining high measurement accuracy to obtain diagnosis based on the fewest amount of analyzed pixels. To reduce imaging time due to the different laser polarizations needed, liquid crystal or electro-optic modulators can be used [64–66], or beams with different polarizations can be interleaved. The clever use of fewer input polarizations could also be used, such as in Stokes-Mueller SHG [67] which uses four polarizations in a PI-SHG setup, or advanced polarimeters with multiple detectors can be used for simultaneous detection of the SHG polarization states [68]. In another technique, polarimetry analysis can also be performed using circularly polarized laser excitation, only requiring a single scan [53, 69]. Fourier techniques could be used for faster data analysis [16, 23, 24], while imaging rates can be increased using higher repetition rate pulsed lasers combined with faster scanners such as spinning mirrors, or by increasing the field of view using a wide-field imaging approach [70]. With these developments, it is reasonable that PSHG microscopy may be implemented in a modified hospital pathology slide scanner. Furthermore, since SHG requires no dyes, it can be implemented as an epi-detection setup in an endoscope for *in vivo* quantitative imaging as a biopsy tool [71–73].

It is evident that PSHG imaging can quantitatively differentiate certain diseased tissues based on their ultrastructure in pathological sample slides however, care must be given to PSHG image quality and the image analysis methods used. For instance, when assessing the quality of PSHG images, it has been found that using SHG intensity as a criterion is only suitable in specific instances [74]. Furthermore, while statistical discrimination based on many samples has been validated in different tissues, the efficacy of diagnosis in individual regions remains unclear and must be addressed. Improved differentiation could be obtained *via* additional implementation of complementary SHG intensity analysis techniques, such as texture analysis [56, 75–77], the Hough transform [78] and the structure tensor [79, 80]. These analysis techniques could be extended to PSHG ρ or δ images. Additional information about diseased tissues can be obtained by coupling complementary techniques, such as polarization-sensitive two-photon excitation fluorescence microscopy [81], and polarization-sensitive third harmonic generation microscopy [82]. The idealized scanning system could find potential hotspots and report them to the pathologist who could confirm the diagnosis, aiding in the difficult task of finding small diseased regions in comparatively large samples, saving pathologists time and lives by pinpointing regions of interest.

AUTHOR CONTRIBUTIONS

The authors contributed to manuscript writing (RC, DT) and editing (RC, AJ, MH, DT).

FUNDING

The research was supported by the Natural Sciences and Engineering Research Council of Canada Discovery Grants Program (RGPIN-2018-05444), Canada's Research Support Fund, and Saint Mary's University.

REFERENCES

1. Kleinman DA. Nonlinear Dielectric Polarization in Optical media. *Phys Rev* (1962) 126:1977–9. doi:10.1103/PhysRev.126.1977
2. Dailey CA, Burke BJ, and Simpson GJ. The General Failure of Kleinman Symmetry in Practical Nonlinear Optical Applications. *Chem Phys Lett* (2004) 390:8–13. doi:10.1016/j.cplett.2004.03.109
3. Roth S, and Freund I. Second Harmonic Generation in Collagen. *J Chem Phys* (1979) 70:1637–43. doi:10.1063/1.437677

4. Roth S, and Freund I. Optical Second-Harmonic Scattering in Rat-Tail Tendon. *Biopolymers* (1981) 20:1271–90. doi:10.1002/bip.1981.360200613
5. Freund I, and Deutsch M. Second-harmonic Microscopy of Biological Tissue. *Opt Lett* (1986) 11:94–6. doi:10.1364/OL.11.000094
6. Freund I, Deutsch M, and Sprecher A. Connective Tissue Polarity. Optical Second-Harmonic Microscopy, Crossed-Beam Summation, and Small-Angle Scattering in Rat-Tail Tendon. *Biophysical J* (1986) 50:693–712. doi:10.1016/S0006-3495(86)83510-X
7. Dick B. Irreducible Tensor Analysis of Sum- and Difference-Frequency Generation in Partially Oriented Samples. *Chem Phys* (1985) 96:199–215. doi:10.1016/0301-0104(85)85085-0
8. Plotnikov SV, Millard AC, Campagnola PJ, and Mohler WA. Characterization of the Myosin-Based Source for Second-Harmonic Generation from Muscle Sarcomeres. *Biophysical J* (2006) 90:693–703. doi:10.1529/biophysj.105.071555
9. Tiaho F, Recher G, and Rouède D. Estimation of Helical Angles of Myosin and Collagen by Second Harmonic Generation Imaging Microscopy. *Opt Express* (2007) 15:12286–95. doi:10.1364/OE.15.012286
10. Tuer AE, Akens MK, Krouglov S, Sandkuijl D, Wilson BC, Whyne CM, et al. Hierarchical Model of Fibrillar Collagen Organization for Interpreting the Second-Order Susceptibility Tensors in Biological Tissue. *Biophysical J* (2012) 103:2093–105. doi:10.1016/j.bpj.2012.10.019
11. Williams RM, Zipfel WR, and Webb WW. Interpreting Second-Harmonic Generation Images of Collagen I Fibrils. *Biophysical J* (2005) 88:1377–86. doi:10.1529/biophysj.104.047308
12. Hompland T, Erikson A, Lindgren M, Lindmo T, and de Lange Davies C. Second-harmonic Generation in Collagen as a Potential Cancer Diagnostic Parameter. *J Biomed Opt* (2008) 13:054050. doi:10.1117/1.2983664
13. Rouède D, Schaub E, Bellanger J-J, Ezan F, Scimeca J-C, Baffet G, et al. Determination of Extracellular Matrix Collagen Fibril Architectures and Pathological Remodeling by Polarization Dependent Second Harmonic Microscopy. *Sci Rep* (2017) 7:12197. doi:10.1038/s41598-017-12398-0
14. Rouède D, Schaub E, Bellanger J-J, Ezan F, and Tiaho F. Wavy Nature of Collagen Fibrils Deduced from the Dispersion of Their Second-Order Nonlinear Optical Anisotropy Parameters ρ. *Opt Express* (2020) 28:4845–58. doi:10.1364/OE.380089
15. Ambekar R, Lau T-Y, Walsh M, Bhargava R, and Toussaint KC. Quantifying Collagen Structure in Breast Biopsies Using Second-Harmonic Generation Imaging. *Biomed Opt Express* (2012) 3:2021–35. doi:10.1364/BOE.3.002021
16. Tsafas V, Gavgiotaki E, Tzardi M, Tsafa E, Fotakis C, Athanassakis I, et al. Polarization-dependent Second-harmonic Generation for Collagen-based Differentiation of Breast Cancer Samples. *J Biophotonics* (2020) 13:e202000180. doi:10.1002/jbio.202000180
17. Matteini P, Cicchi R, Ratto F, Kapsokalyvas D, Rossi F, de Angelis M, et al. Thermal Transitions of Fibrillar Collagen Unveiled by Second-Harmonic Generation Microscopy of Corneal Stroma. *Biophysical J* (2012) 103:1179–87. doi:10.1016/j.bpj.2012.07.055
18. Lin J, Pan S, Zheng W, and Huang Z. Polarization-resolved Second-Harmonic Generation Imaging for Liver Fibrosis Assessment without Labeling. *Appl Phys Lett* (2013) 103:173701. doi:10.1063/1.4826516
19. Brown CP, Houle M-A, Popov K, Nicklaus M, Couture C-A, Laliberté M, et al. Imaging and Modeling Collagen Architecture from the Nano to Micro Scale. *Biomed Opt Express* (2014) 5:233–43. doi:10.1364/boe.5.000233
20. Ávila FJ, Del Barco O, and Bueno JM. Polarimetric Multiphoton Microscopy for the Analysis of Ocular Structures. *Opt Pura Apl* (2019) 52:1–9. doi:10.7149/OPA.52.1.51013
21. Raoux C, Schmeltz M, Bied M, Alnawaiseh M, Hansen U, Latour G, et al. Quantitative Structural Imaging of Keratoconic Corneas Using Polarization-Resolved SHG Microscopy. *Biomed Opt Express* (2021) 12:4163–78. doi:10.1364/boe.426145
22. Amat-Roldan I, Psilodimitrakopoulos S, Loza-Alvarez P, and Artigas D. Fast Image Analysis in Polarization SHG Microscopy. *Opt Express* (2010) 18:17209–19. doi:10.1364/OE.18.017209
23. Alizadeh M, Merino D, Lombardo G, Lombardo M, Mencucci R, Ghotbi M, et al. Identifying Crossing Collagen Fibers in Human Corneal Tissues Using pSHG Images. *Biomed Opt Express* (2019) 10:3875–88. doi:10.1364/boe.10.003875
24. Mercatelli R, Triulzi T, Pavone FS, Orlandi R, and Cicchi R. Collagen Ultrastructural Symmetry and its Malignant Alterations in Human Breast Cancer Revealed by Polarization-resolved Second-harmonic Generation Microscopy. *J Biophotonics* (2020) 13:e202000159. doi:10.1002/jbio.202000159
25. Quigley AS, Bancelin S, Deska-Gauthier D, Légaré F, Kreplak L, and Veres SP. In Tendons, Differing Physiological Requirements lead to Functionally Distinct Nanostructures. *Sci Rep* (2018) 8:4409. doi:10.1038/s41598-018-22741-8
26. Duboisset J, Aït-Belkacem D, Roche M, Rigneault H, and Brasselet S. Generic Model of the Molecular Orientational Distribution Probed by Polarization-Resolved Second-Harmonic Generation. *Phys Rev A* (2012) 85:043829. doi:10.1103/PhysRevA.85.043829
27. Mansfield JC, Mandalia V, Toms A, Winlove CP, and Brasselet S. Collagen Reorganization in Cartilage under Strain Probed by Polarization Sensitive Second Harmonic Generation Microscopy. *J R Soc Interface* (2019) 16:20180611. doi:10.1098/rsif.2018.0611
28. Aït-Belkacem D, Guilbert M, Roche M, Duboisset J, Ferrand P, Sockalingum G, et al. Microscopic Structural Study of Collagen Aging in Isolated Fibrils Using Polarized Second Harmonic Generation. *J Biomed Opt* (2012) 17:080506. doi:10.1117/1.JBO.17.8.080506
29. Wang J-Y, Mansfield JC, Brasselet S, Vergari C, Meakin JR, and Winlove CP. Micro-mechanical Damage of Needle Puncture on Bovine Annulus Fibrosus Fibrils Studied Using Polarization-Resolved Second Harmonic Generation(P-SHG) Microscopy. *J Mech Behav Biomed Mater* (2021) 118:104458. doi:10.1016/j.jmbbm.2021.104458
30. Yasui T, Takahashi Y, Fukushima S, Ogura Y, Yamashita T, Kuwahara T, et al. Observation of Dermal Collagen Fiber in Wrinkled Skin Using Polarization-Resolved Second-Harmonic-Generation Microscopy. *Opt Express* (2009) 17:912–23. doi:10.1364/oe.17.000912
31. Fukushima S-i., Yonetsu M, and Yasui T. Polarization-resolved Second-Harmonic-Generation Imaging of Dermal Collagen Fiber in Prewrinkled and Wrinkled Skins of Ultraviolet-B-Exposed Mouse. *J Biomed Opt* (2018) 24:031006. doi:10.1117/1.JBO.24.3.031006
32. Tanaka Y, Hase E, Fukushima S, Ogura Y, Yamashita T, Hirao T, et al. Motion-artifact-robust, Polarization-Resolved Second-Harmonic-Generation Microscopy Based on Rapid Polarization Switching with Electro-Optic Pockells Cell and its Application to *In Vivo* Visualization of Collagen Fiber Orientation in Human Facial Skin. *Biomed Opt Express* (2014) 5:1099–113. doi:10.1364/boe.5.001099
33. Hristu R, Stanciu SG, Tranca DE, and Stanciu GA. Improved Quantification of Collagen Anisotropy with Polarization-Resolved Second Harmonic Generation Microscopy. *J Biophoton* (2017) 10:1171–9. doi:10.1002/jbio.201600197
34. Miler I, Rabasovic MD, Aleksic M, Krmpot AJ, Kalezic A, Jankovic A, et al. Polarization-resolved SHG Imaging as a Fast Screening Method for Collagen Alterations during Aging: Comparison with Light and Electron Microscopy. *J Biophotonics* (2021) 14:e202000362. doi:10.1002/jbio.202000362
35. Nadiarnykh O, Plotnikov S, Mohler WA, Kalajzic I, Redford-Badwal D, and Campagnola PJ. Second Harmonic Generation Imaging Microscopy Studies of Osteogenesis Imperfecta. *J Biomed Opt* (2007) 12:051805. doi:10.1117/1.2799538
36. Birk JW, Tadros M, Moezardalan K, Nadyarnykh O, Forouhar F, Anderson J, et al. Second Harmonic Generation Imaging Distinguishes Both High-Grade Dysplasia and Cancer from normal Colonic Mucosa. *Dig Dis Sci* (2014) 59:1529–34. doi:10.1007/s10620-014-3121-7
37. Nadiarnykh O, LaComb RB, Brewer MA, and Campagnola PJ. Alterations of the Extracellular Matrix in Ovarian Cancer Studied by Second Harmonic Generation Imaging Microscopy. *BMC Cancer* (2010) 10:1471–2407. doi:10.1186/1471-2407-10-94
38. Gusachenko I, Tran V, Houssen YG, Allain J-M, and Schanne-Klein M-C. Polarization-resolved Second-Harmonic Generation in Tendon upon Mechanical Stretching. *Biophysical J* (2012) 102:2220–9. doi:10.1016/j.bpj.2012.03.068
39. Silva DFT, Gomes ASL, De Campos Vidal B, and Ribeiro MS. Birefringence and Second Harmonic Generation on Tendon Collagen Following Red Linearly Polarized Laser Irradiation. *Ann Biomed Eng* (2013) 41:752–62. doi:10.1007/s10439-012-0720-3

40. Radaelli F, D'Alfonso L, Collini M, Mingozzi F, Marongiu L, Granucci F, et al. μMAPPS: a Novel Phasor Approach to Second Harmonic Analysis for In Vitro-In Vivo Investigation of Collagen Microstructure. *Sci Rep* (2017) 7: 17468. doi:10.1038/s41598-017-17726-y
41. Scodellaro R, Bouzin M, Mingozzi F, D'Alfonso L, Granucci F, Collini M, et al. Whole-Section Tumor Micro-architecture Analysis by a Two-Dimensional Phasor-Based Approach Applied to Polarization-dependent Second Harmonic Imaging. *Front Oncol* (2019) 9:527. doi:10.3389/fonc.2019.00527
42. Chen W-C, Chen Y-J, Lin S-T, Hung W-H, Chan M-C, Wu I-C, et al. Label-free Characterization of Collagen Fibers in Cancerous Esophagus Tissues Using Ratiometric Nonlinear Optical Microscopy. *Exp Biol Med (Maywood)* (2020) 245:1213–21. doi:10.1177/1535370220934039
43. Chen X, Raggio C, and Campagnola PJ. Second-harmonic Generation Circular Dichroism Studies of Osteogenesis Imperfecta. *Opt Lett* (2012) 37:3837–9. doi:10.1364/OL.37.003837
44. Golaraei A, Kontenis L, Cisek R, Tokarz D, Done SJ, Wilson BC, et al. Changes of Collagen Ultrastructure in Breast Cancer Tissue Determined by Second-Harmonic Generation Double Stokes-Mueller Polarimetric Microscopy. *Biomed Opt Express* (2016) 7:4054–68. doi:10.1364/BOE.7.004054
45. Campbell KR, and Campagnola PJ. Wavelength-Dependent Second Harmonic Generation Circular Dichroism for Differentiation of Col I and Col III Isoforms in Stromal Models of Ovarian Cancer Based on Intrinsic Chirality Differences. *J Phys Chem B* (2017) 121:1749–57. doi:10.1021/acs.jpcb.6b06822
46. Golaraei A, Kontenis L, Mirsanaye K, Krouglov S, Akens MK, Wilson BC, et al. Complex Susceptibilities and Chiroptical Effects of Collagen Measured with Polarimetric Second-Harmonic Generation Microscopy. *Sci Rep* (2019) 9: 12488. doi:10.1038/s41598-019-48636-w
47. James DS, Jambor AN, Chang H-Y, Alden Z, Tilbury KB, Sandbo NK, et al. Probing ECM Remodeling in Idiopathic Pulmonary Fibrosis via Second Harmonic Generation Microscopy Analysis of Macro/supramolecular Collagen Structure. *J Biomed Opt* (2019) 25:014505. doi:10.1117/1.jbo.25.1.014505
48. James DS, Brereton CJ, Davies DE, Jones MG, and Campagnola PJ. Examining Lysyl Oxidase-like Modulation of Collagen Architecture in 3D Spheroid Models of Idiopathic Pulmonary Fibrosis via Second-Harmonic Generation Microscopy. *J Biomed Opt* (2021) 26:066501. doi:10.1117/1.jbo.26.6.066501
49. Campbell KR, Chaudhary R, Handel JM, Patankar MS, and Campagnola PJ. Polarization-resolved Second Harmonic Generation Imaging of Human Ovarian Cancer. *J Biomed Opt* (2018) 23:066501. doi:10.1117/1.JBO.23.6.066501
50. Samim M, Krouglov S, and Barzda V. Double Stokes Mueller Polarimetry of Second-Harmonic Generation in Ordered Molecular Structures. *J Opt Soc Am B* (2015) 32:451–60. doi:10.1364/JOSAB.32.000451
51. Samim M, Krouglov S, and Barzda V. Nonlinear Stokes-Mueller Polarimetry. *Phys Rev A* (2016) 93:013847. doi:10.1103/PhysRevA.93.013847
52. Tuer AE, Krouglov S, Prent N, Cisek R, Sandkuijl D, Yasufuku K, et al. Nonlinear Optical Properties of Type I Collagen Fibers Studied by Polarization Dependent Second Harmonic Generation Microscopy. *J Phys Chem B* (2011) 115:12759–69. doi:10.1021/jp206308k
53. Alizadeh M, Ghotbi M, Loza-Alvarez P, and Merino D. Comparison of Different Polarization Sensitive Second Harmonic Generation Imaging Techniques. *Methods Protoc* (2019) 2:49. doi:10.3390/mps2020049
54. Golaraei A, Mirsanaye K, Ro Y, Krouglov S, Akens MK, Wilson BC, et al. Collagen Chirality and Three-Dimensional Orientation Studied with Polarimetric Second-Harmonic Generation Microscopy. *J Biophotonics* (2019) 12:e201800241. doi:10.1002/jbio.201800241
55. Tokarz D, Cisek R, Golaraei A, Asa SL, Barzda V, and Wilson BC. Ultrastructural Features of Collagen in Thyroid Carcinoma Tissue Observed by Polarization Second Harmonic Generation Microscopy. *Biomed Opt Express* (2015) 6:3475–81. doi:10.1364/BOE.6.003475
56. Golaraei A, Mostaço-Guidolin LB, Raja V, Navab R, Wang T, Sakashita S, et al. Polarimetric Second-Harmonic Generation Microscopy of the Hierarchical Structure of Collagen in Stage I-III Non-small Cell Lung Carcinoma. *Biomed Opt Express* (2020) 11:1851–63. doi:10.1364/boe.387744
57. Golaraei A, Cisek R, Krouglov S, Navab R, Niu C, Sakashita S, et al. Characterization of Collagen in Non-small Cell Lung Carcinoma with Second Harmonic Polarization Microscopy. *Biomed Opt Express* (2014) 5: 3562–7. doi:10.1364/BOE.5.003562
58. Tokarz D, Cisek R, Golaraei A, Krouglov S, Navab R, Niu C, et al. Tumor Tissue Characterization Using Polarization-Sensitive Second Harmonic Generation Microscopy. *Proceed SPIE* (2015) 9531:95310C. doi:10.1117/12.2180969
59. Tokarz D, Cisek R, Joseph A, Asa SL, Wilson BC, and Barzda V. Characterization of Pathological Thyroid Tissue Using Polarization-Sensitive Second Harmonic Generation Microscopy. *Lab Invest* (2020) 100: 1280–7. doi:10.1038/s41374-020-0475-7
60. Tokarz D, Cisek R, Joseph A, Golaraei A, Mirsanaye K, Krouglov S, et al. Characterization of Pancreatic Cancer Tissue Using Multiphoton Excitation Fluorescence and Polarization-Sensitive Harmonic Generation Microscopy. *Front Oncol* (2019) 9:272. doi:10.3389/fonc.2019.00272
61. Burke M, Golaraei A, Atkins A, Akens M, Barzda V, and Whyne C. Collagen Fibril Organization within Rat Vertebral Bone Modified with Metastatic Involvement. *J Struct Biol* (2017) 199:153–64. doi:10.1016/j.jsb.2017.06.008
62. Han X, Burke RM, Zettel ML, Tang P, and Brown EB. Second Harmonic Properties of Tumor Collagen: Determining the Structural Relationship between Reactive Stroma and Healthy Stroma. *Opt Express* (2008) 16: 1846–59. doi:10.1364/oe.16.001846
63. Doras C, Taupier G, Barsella A, Mager L, Boeglin A, Bulou H, et al. Polarization State Studies in Second Harmonic Generation Signals to Trace Atherosclerosis Lesions. *Opt Express* (2011) 19:15062–8. doi:10.1364/oe.19.015062
64. Dewalt EL, Sullivan SZ, Schmitt PD, Muir RD, and Simpson GJ. Polarization-modulated Second Harmonic Generation Ellipsometric Microscopy at Video Rate. *Anal Chem* (2014) 86:8448–56. doi:10.1021/ac502124v
65. Dow XY, DeWalt EL, Sullivan SZ, Schmitt PD, Ulcickas JRW, and Simpson GJ. Imaging the Nonlinear Susceptibility Tensor of Collagen by Nonlinear Optical Stokes Ellipsometry. *Biophysical J* (2016) 111:1361–74. doi:10.1016/j.bpj.2016.05.055
66. Reiser K, Stoller P, and Knoesen A. Three-Dimensional Geometry of Collagenous Tissues by Second Harmonic Polarimetry. *Sci Rep* (2017) 7: 2642. doi:10.1038/s41598-017-02326-7
67. Ávila FJ, Del Barco O, and Bueno JM. Quantifying External and Internal Collagen Organization from Stokes-Vector-Based Second Harmonic Generation Imaging Polarimetry. *J Opt* (2017) 19:105301. doi:10.1088/2040-8986/aa825d
68. Mazumder N, Qiu J, Foreman MR, Romero CM, Hu C-W, Tsai H-R, et al. Polarization-resolved Second Harmonic Generation Microscopy with a Four-Channel Stokes-Polarimeter. *Opt Express* (2012) 20:14090–9. doi:10.1364/OE.20.014090
69. Psilodimitrakopoulos S, Loza-Alvarez P, and Artigas D. Fast Monitoring of Iin-Vvivo Conformational Changes in Myosin Using Single Scan Polarization-SHG Microscopy. *Biomed Opt Express* (2014) 5:4362–73. doi:10.1364/BOE.5.004362
70. Zhao H, Cisek R, Karunendiran A, Tokarz D, Stewart BA, and Barzda V. Live Imaging of Contracting Muscles with Wide-Field Second Harmonic Generation Microscopy Using a High Power Laser. *Biomed Opt Express* (2019) 10:5130–5. doi:10.1364/boe.10.005130
71. Fu L, and Gu M. Polarization Anisotropy in Fiber-Optic Second Harmonic Generation Microscopy. *Opt Express* (2008) 16:5000–6. doi:10.1364/oe.16.005000
72. Bao H, Boussioutas A, Jeremy R, Russell S, and Gu M. Second Harmonic Generation Imaging via Nonlinear Endomicroscopy. *Opt Express* (2010) 18: 1255–60. doi:10.1364/oe.18.001255
73. Ducourthial G, Leclerc P, Mansuryan T, Fabert M, Brevier J, Habert R, et al. Development of a Real-Time Flexible Multiphoton Microendoscope for Label-free Imaging in a Live Animal. *Sci Rep* (2015) 5:18303. doi:10.1038/srep18303
74. Stanciu SG, Ávila FJ, Hristu R, and Bueno JM. A Study on Image Quality in Polarization-Resolved Second Harmonic Generation Microscopy. *Sci Rep* (2017) 7:15476. doi:10.1038/s41598-017-15257-0
75. Pouli D, Genega EM, Sullivan TB, Rieger-Christ KM, Wright V, Georgakoudi I, et al. Two-photon Images Reveal Unique Texture Features for Label-free Identification of Ovarian Cancer Peritoneal Metastases. *Biomed Opt Express* (2019) 10:4479–88. doi:10.1364/boe.10.004479
76. Mostaço-Guidolin LB, Osei ET, Ullah J, Hajimohammadi S, Fouadi M, Li X, et al. Defective Fibrillar Collagen Organization by Fibroblasts Contributes to

Airway Remodeling in Asthma. *Am J Respir Crit Care Med* (2019) 200:431–43. doi:10.1164/rccm.201810-1855OC

77. Gant KL, Jambor AN, Li Z, Rentchler EC, Weisman P, Li L, et al. Evaluation of Collagen Alterations in Early Precursor Lesions of High Grade Serous Ovarian Cancer by Second Harmonic Generation Microscopy and Mass Spectrometry. *Cancers* (2021) 13:2794. doi:10.3390/cancers13112794
78. Bueno JM, Ávila FJ, Hristu R, Stanciu SG, Eftimie L, and Stanciu GA. Objective Analysis of Collagen Organization in Thyroid Nodule Capsules Using Second Harmonic Generation Microscopy Images and the Hough Transform. *Appl Opt* (2020) 59:6925–31. doi:10.1364/ao.393721
79. Ávila FJ, and Bueno JM. Analysis and Quantification of Collagen Organization with the Structure Tensor in Second Harmonic Microscopy Images of Ocular Tissues. *Appl Opt* (2015) 54:9848–54. doi:10.1364/AO.54.009848
80. Bueno JM, Ávila FJ, and Martínez-García MC. Quantitative Analysis of the Corneal Collagen Distribution after *In Vivo* Cross-Linking with Second Harmonic Microscopy. *Biomed Res Int* (2019) 2019:3860498. doi:10.1155/2019/3860498
81. Artigas D, Merino D, Polzer C, and Loza-Alvarez P. Sub-diffraction Discrimination with Polarization-Resolved Two-Photon Excited Fluorescence Microscopy. *Optica* (2017) 4:911–8. doi:10.1364/optica.4.000911
82. Morizet J, Ducourthial G, Supatto W, Boutillon A, Legouis R, Schanne-Klein M-C, et al. High-speed Polarization-Resolved Third-Harmonic Microscopy. *Optica* (2019) 6:385–8. doi:10.1364/OPTICA.6.000385

Conflict of Interest: The authors declare that the research was conducted in the absence of any commercial or financial relationships that could be construed as a potential conflict of interest.

Publisher's Note: All claims expressed in this article are solely those of the authors and do not necessarily represent those of their affiliated organizations, or those of the publisher, the editors and the reviewers. Any product that may be evaluated in this article, or claim that may be made by its manufacturer, is not guaranteed or endorsed by the publisher.